

A Three-rhombus Configured Remote Center of Motion Mechanism for Robot-assisted Surgery

Yuzhou Duan, Yunzhi Zhang, Yayi Shen, Jie Ling* and Yuchuan Zhu

College of Mechanical & Electrical Engineering, Nanjing University of Aeronautics and Astronautics, Nanjing 210016, China

* Email: meejling@nuaa.edu.cn

Abstract—Remote center of motion (RCM) mechanisms are widely utilized to achieve minimally invasive surgery (MIS) instead of manual operation. To realize the translation motion in an RCM mechanism, the proximal actuation method is generally adopted, which has the disadvantages of reducing the vision field, offsetting the RCM point, and increasing the moment of inertia. This paper proposes a surgery robot with a novel RCM configuration realized by a three-rhombus mechanism. The great merit of this robot is the actuators are all mounted on the base. The kinematics and singularity of the mechanism are investigated analytically. Parameter optimization is done under the given rotation angle of 90° and feed depth of 47.8 mm, respectively. Preliminary simulations are conducted in SolidWorks environment to validate the effectiveness of the RCM mechanism.

Index Terms—Remote center motion, Minimally invasive surgery, Kinematics analysis.

I. INTRODUCTION

Robot-assisted surgery is becoming more and more popular in the medical field with the advantages of flexibility, accuracy, and stability [1]. Compared with open surgery, minimally invasive surgery (MIS) has the advantages of shorter hospital stay and less blood loss [2]. As shown in Fig. 1, the surgical instrument (end effectors) is limited in the interactive point of the human body during the MIS surgery process. Therefore, the end effector has only four degrees of freedom (DOFs), i.e., three rotation (3R) DOFs and one translation (1T) DOF. The motion of the end effector forms a remote center of motion (RCM), while the interactive point is called the RCM point [3]. In general, there are two main ways to realize an RCM: active constrains [4], [5] and passive constrains [6], [7]. As for the active constrain, it always requires control algorithms to form a virtual RCM point, hence it is less safe during a surgery process. This paper adopts the passive constrain (or physical constrain) to restrict the motion of the end effector and to form the RCM point structurally.

Circular rail, double-parallelogram, serial spherical, and parallel spherical are four types of 1-DOF RCM modules widely used in MIS robots [8] to conduct 1R motion. Considering high rigidity, a dual trigonometric-ratio-based RCM module is proposed in [9]. Aiming at expanding the working

This work was supported by Natural Science Foundation of Jiangsu Province (Grant No. BK20210294), and the National Undergraduate Innovation and Entrepreneurship Program (Grant No. 202110287128Y).

Corresponding author: Jie Ling.

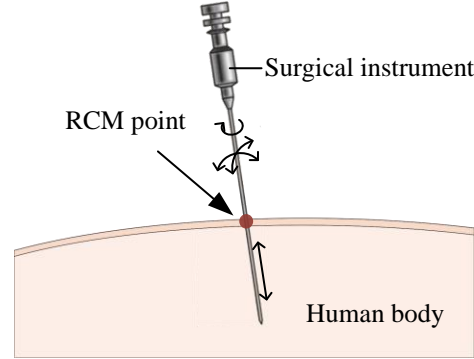


Fig. 1. Schematics of the MIS and the DOFs of the surgical instrument.

space, a new RCM module using spherical scissor linkages is developed in [10] to form an entire hemisphere working space. Most of the time, to realize the 3R1T motion, the 1R and 1T modules are connected in series [11], [12]. Therefore, a linear actuator is supposed to be added near the end effector (proximal actuation). Nevertheless, this kind of actuation has the following disadvantages:

- The installation of proximal motor will increase the mechanism deflection and offset the RCM point.
- The proximal actuation method occupies too much volume near the end, which reduces the vision field of surgeons as well as the operating space.
- The proximal motor increases the moment of inertia near the end, further increasing power consumption and decreasing structure natural frequency.

Many efforts have been made to address the proximal actuation problem. An approach to construct 1R1T RCM mechanisms inspired by the pantograph mechanisms is proposed in [13]. The motion of a traditional 1R1T mechanism is copied by different pantograph mechanisms and then repeated in the remote space. However, the structure of the pantograph mechanisms is too complex to realize the repetition of the 1R1T motion, which raises the risk of collision and decreases rigidity. A base-actuated 1R1T close-loop mechanism by using parallelogram mechanism is developed in [14], while the parallelogram-based mechanism occupies much working space and has relatively low stiffness. The method of cable transmissions is also adopted to avoid the proximal actuation [15].

Several coupled cable transmissions are utilized to constrain a serial kinematic chain. But this method has low load capacity and transmission efficiency.

Inspired by the method of “virtual center” (VC) [13], in this paper, the so-called three-rhombus RCM mechanism is developed, which has two planar DOFs, i.e., one rotation and one translation. The proposed mechanism realizes the RCM by the three-rhombus structure. The main merit of the proposed mechanism lies in that all the actuators are mounted on the base. This configuration avoids the disadvantages of reducing the vision field, offsetting the RCM point, and increasing the moment of inertia. Both the forward and the inverse kinematics of the proposed RCM mechanism are established and then the Jacobian matrices of the mechanism are derived. Based on the proposed analytical models, the singularity and the working space of the mechanism are analyzed. Parameter optimization is conducted based on the rotation angle and feed depth. Preliminary simulations with optimized parameters are done to validate the effectiveness of the mechanism.

The rest of this paper is organized as follows. Section II presents the conceptual design of the three-rhombus RCM mechanism. Kinematics and Jacobian matrices are analytically modeled in Section III. In Section IV, the singularity and the working space of the mechanism are both analyzed and the parameters of the mechanism are optimized. In Section V, simulation is done to validate the models and the working space. Results are discussed and conclusions are drawn in Section VI.

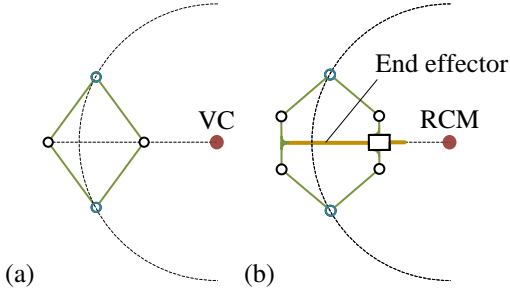


Fig. 2. Schematics of the sub-mechanism inspired by the constrained four-linkage rhombus structure. (a) The constrained four-linkage rhombus structure. The motion of the two diagonal points is on an arc centered on the VC. (b) The sub-mechanism. The end effector on it has a two DOFs planar RCM.

II. CONCEPTUAL DESIGN

In this section, the characteristics of the four-linkage rhombus structure with different constraints are analyzed and assembled to form the three-rhombus mechanism.

Considering a four-linkage rhombus mechanism in Fig. 2(a). The motions of the two points on the diagonal of the rhombus mechanism are assumed to be independently constrained to an arc centered on the virtual center (VC). Due to the perpendicular relationship between two diagonal lines of the rhombus mechanism, one of them always crosses the VC. Based on this principle, in Fig. 2(b), a two DOF sub-mechanism is proposed, where the end effector is always

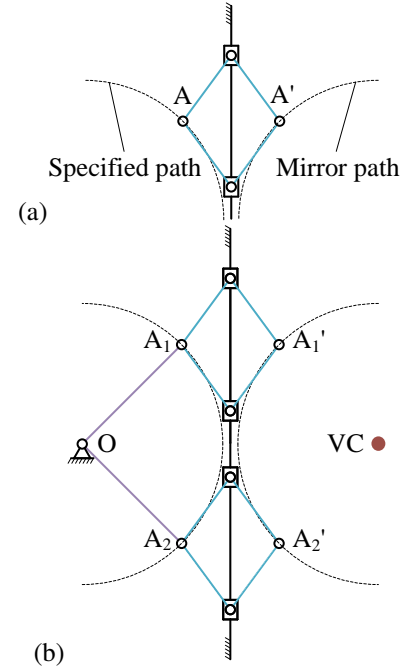


Fig. 3. Schematics of the sub-mechanism inspired by the constrained four-linkage rhombus structure. (a) The constrained four-linkage rhombus structure. Point A' produces a mirror path under the specified path of point A. (b) The sub-mechanism. The mirror motion of point A'_1 and A'_2 has a common VC.

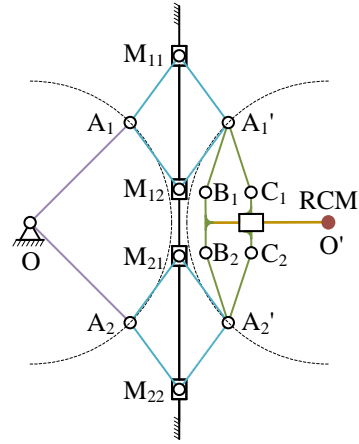


Fig. 4. Schematics of the proposed three-rhombus RCM mechanism.

perpendicular to one of the diagonal line. When two points are constrained to the arc rotating around the RCM in the same direction with the same speed, the end effector has a rotation motion around the RCM. When the points rotates in the opposite direction with the same speed, the end effector has a translation motion along the end effector.

For the four-linkage rhombus mechanism in Fig. 3(a), the two points on the diagonal of the rhombus mechanism are connected with the same prismatic pair. In that case, specify a path at point A, the path of point A' is the mirror path of Point A. Then, the sub-mechanism in Fig. 3(b) is obtained, constrained by linkage OA₁ and OA₂ respectively, the motion of point A₁ and A₂ is on the arc centered on point O, so the

mirror motion of point A'_1 and A'_2 has a common VC.

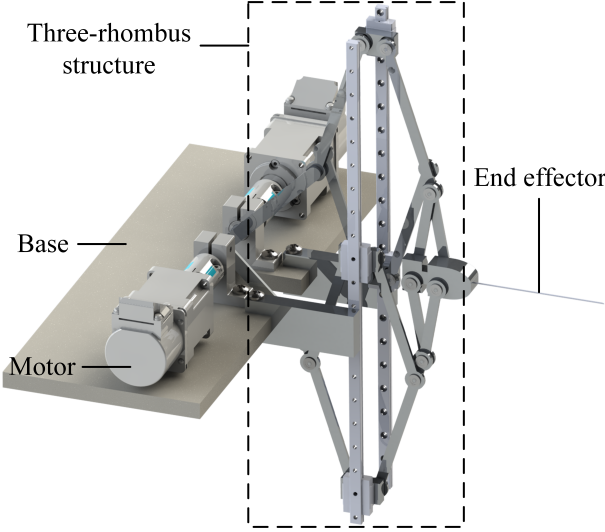


Fig. 5. 3D model of the three-rhombus mechanism.

As shown in Fig. 4, by combining the sub-mechanisms in Fig. 2(b) and Fig. 3(b), the so-called three-rhombus RCM mechanism is obtained, which has two planar DOFs. OA_1 and OA_2 are the active linkages. In addition, the feed motion and the rotation motion of the end effector can be decoupled: when the two linkages rotate in the same direction with the same speed, the end effector has a rotation motion. When the two linkages rotate in the opposite direction with the same speed, the end effector has a translation motion. The two motion patterns are analytically validated in section III.

The three-dimensional model is established as shown in Fig. 5. Two motors and the linear guiders of the three-rhombus structure are all mounted on the base. In this model, 9 gauge spinal needle are adopted as the end effector.

TABLE I
PARAMETERS OF THE LINKAGES OF THE PROPOSED MECHANISM.

Linkage	Parameter
OA_1, OA_2	l_1
A_iM_{ij}, A'_iM_{ij} ($i = 1, 2; j = 1, 2$)	l_2
$A'_1B_1, A'_2B_2, A'_1C_1, A'_2C_2$	l_3
B_1B_2, C_1C_2	l_4
end effector	l_5

III. KINEMATICS MODELING

In this section, both the forward and inverse kinematics of the three-rhombus mechanism are established. The parameters of the linkages are listed in TABLE I.

A. Forward Kinematics

For a planar RCM mechanism applied in MIS. The output is typically denoted by the rotation angle and the feed depth of the end effector. As shown in Fig. 6, the linkage OA_1 and OA_2 are the two active linkages. θ_1 and θ_2 are the input variables

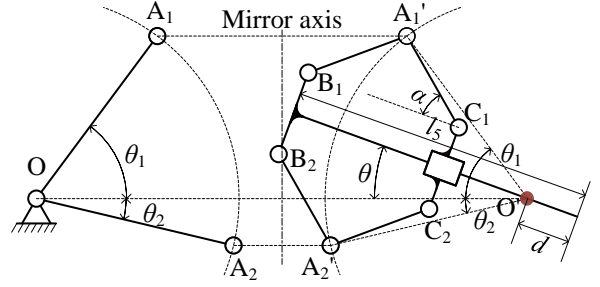


Fig. 6. Kinematic structure of the three-rhombus mechanism

of the mechanism. Since the point A_1 and A_2 rotate around O , the mirror point A'_1 and A'_2 rotate around O' . The orientation of the end effector can be directly obtained as

$$\theta = \frac{1}{2}(\theta_1 + \theta_2) \quad (1)$$

where θ is the rotation angle of the end effector represented by the acute angle between line OO' and the end effector. Counterclockwise is positive for θ_1 and θ_2 .

By solving a simple geometry problem, the feed depth of the end effector can be represented as follows

$$d = l_5 - l_3 \cos \alpha - l_1 \cos\left(\frac{\theta_1 - \theta_2}{2}\right) \quad (2)$$

where, d is the feed depth represented by the displacement of the RCM point O' with respect to the tip of the end effector on its axis direction. α is the acute angle between lines A'_1C_1 and B_1C_1 , which takes the form

$$\alpha = \arcsin\left(\frac{1}{l_3}\left(l_1 \sin\left(\frac{\theta_1 - \theta_2}{2}\right) - \frac{l_4}{2}\right)\right) \quad (3)$$

B. Inverse Kinematics

By performing simple mathematical operations on (1) (3), the inverse kinematics can be written as follows

$$\begin{cases} \theta_1 = \theta + \Delta \\ \theta_2 = \theta - \Delta \end{cases} \quad (4)$$

where

$$\begin{cases} d_0 = l_5 - d \\ c = d_0^2 + l_1^2 - l_3^2 + \frac{l_4^2}{4} \\ \Delta = \arccos\left(\frac{c}{l_1 \sqrt{4d_0^2 + l_4^2}}\right) + \arctan\left(\frac{l_4}{2d_0}\right) \end{cases} \quad (5)$$

Equation (5) represents that Δ is the function of d . From (4) it can be conclude that the output θ and d can be decoupled by the inputs $\frac{\theta_1 + \theta_2}{2}$ and $\frac{\theta_1 - \theta_2}{2}$, i.e., when linkages OA_1 and OA_2 rotate in the same direction with the same speed, the end effector has a rotation motion. When the two linkages rotate in the opposite direction with the same speed, the end effector has a translation motion.

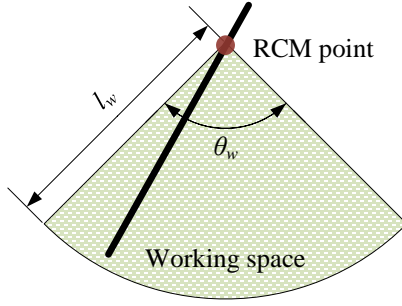


Fig. 7. Schematics of the MIS and the DOFs of the surgical instrument.

C. Jacobian Matrix

The relationship between the input variables and the output variables can be written as

$$\mathbf{F}(\mathbf{x}, \boldsymbol{\theta}) = 0 \quad (6)$$

where $\mathbf{x} = [\theta, d_0]'$, $\boldsymbol{\theta} = [\theta_1, \theta_2]'$.

Differentiating (6) respect to time leads the following equation

$$\mathbf{A}\dot{\mathbf{x}} + \mathbf{B}\dot{\boldsymbol{\theta}} = 0 \quad (7)$$

where

$$\mathbf{A} = \frac{\partial \mathbf{F}}{\partial \mathbf{x}}, \mathbf{B} = \frac{\partial \mathbf{F}}{\partial \boldsymbol{\theta}}. \quad (8)$$

Based on the kinematic results, substitution of (1) (2) (3) into (7) gives

$$\mathbf{A} = \begin{bmatrix} -2 & 0 \\ 0 & -2 \end{bmatrix}, \mathbf{B} = \begin{bmatrix} 1 & 1 \\ \lambda & -\lambda \end{bmatrix} \quad (9)$$

where \mathbf{A} and \mathbf{B} are both Jacobian matrices. The parameter λ takes the form

$$\lambda = l_1 \sin\left(\frac{\theta_1 - \theta_2}{2}\right) + l_1 \tan(\alpha) \cos\left(\frac{\theta_1 - \theta_2}{2}\right) \quad (10)$$

IV. ANALYSIS AND OPTIMIZATION

A. Singularity analysis

Singularity occurs either \mathbf{A} or \mathbf{B} becomes singular. In this mechanism, singularity occurs only when

$$\det(\mathbf{B}) = 0. \quad (11)$$

Substitution of (9) (10) into (11) gives

$$\sin\left(\frac{\theta_1 - \theta_2}{2}\right) = \frac{l_4}{2(l_1 - l_3)} = \sin(\alpha). \quad (12)$$

B. Working Space Analysis

Limited by the structure as well as to get better kinematics, α satisfies

$$\alpha \geq \alpha_1, \alpha \leq \alpha_2 \quad (13)$$

where, α_1 and α_2 are respect to the kinematic characteristics. And to avoid singularity, according to (12), the restriction can be written as follows:

$$\alpha_1 \geq \arcsin\left(\frac{l_4}{2(l_1 - l_3)}\right) \quad (14)$$

As discussed above, the two DOFs of the end effector denoted by feed depth d and rotation angle θ are decoupled. So the working space is supposed to be a sector (Fig. 7), which can be easily represented as

$$l_w = \kappa_1 - \kappa_2 \quad (15)$$

$$\theta_w = \pi - 2\arcsin\left(\frac{l_3 \sin \alpha_2 + \frac{l_4}{2}}{l_1}\right) \quad (16)$$

where, l_w and θ_w are the radius and the arc angle of the sector, respectively. The parameters κ_i ($i = 1, 2$) take the form

$$\kappa_i = \sqrt{l_1^2 - (l_3 \sin \alpha_i + \frac{l_4}{2})^2} - l_3 \sin \alpha_i \quad (16)$$

TABLE II
VALUES OF THE CONSTANT PARAMETERS FOR OPTIMIZATION AND
OPTIMIZED PARAMETERS.

Parameter	Value	Parameter	Value
l_1	70.64 mm	l_5	115.5 mm
l_3	46.66 mm	α_1	10°
l_4	8 mm	α_2	80°
l_d	47.8 mm	θ_d	90°

C. Optimization

According from (15), the working space of the mechanism can be determined by the following five parameters: $l_1, l_3, l_4, \alpha_1, \alpha_2$. α_1 and α_2 can be determined by the desired mechanical characteristics. l_4 is respect to the volume of the end effector. So the working space can be determined by l_1 and l_3 .

The end effector is loaded when the RCM mechanism is operating, which causes deformation of the mechanism and further offsetting the RCM point. So the stiffness of the RCM mechanism is a considerable issue.

Optimization design has been carried out to improve the stiffness of the structure under the specific working space, which can be concluded as follows:

- Objective: To increase stiffness, minimize the value of l_3 .
- Related parameters: l_1 and l_3
- Constraint condition: 1) The working space must be larger than the desired one. 2) The singularity needs to be avoided in the working space.

The mathematical version of the constraint condition is represented as follows:

$$\text{s.t. } \begin{cases} \theta_w \geq \theta_d \\ l_w \geq l_d \\ \alpha_1 \geq \arcsin\left(\frac{l_4}{2(l_1 - l_3)}\right) \end{cases} \quad (17)$$

where, θ_w and l_w represented the desired sector-shaped working space. One group of typical value of the constant parameters are selected in TABLE II. The parameters are determined by the needs of spinal anesthesia. By using Matlab Optimization toolbox with the appropriate initial value $[l_1, l_3] = [150, 60]$, the optimized values of l_1 and l_3 is also listed in TABLE II.

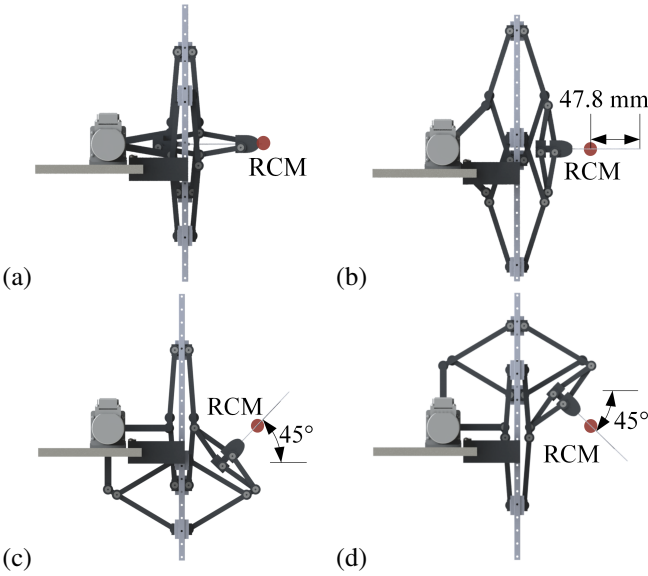


Fig. 8. Working space and RCM verification of the developed three-rhombus mechanism. (a) The initial configuration and the RCM point. (b) the maximum feed depth of the mechanism (47.8 mm). (c) The lower limit of the rotation angle (45°). (d) The upper limit of the rotation angle (45°).

V. SIMULATIONS

In Section IV, the parameters of the three-rhombus RCM mechanism are optimized. The CAD model of the mechanism is established to preliminary validate the working space as well as the working space.

A. Simulation Setup

The kinematic simulation is conducted in SolidWorks environment. To ensure the working space, the relationship that $l_2 > l_1$ needs to be satisfied. In this paper, to avoid the risk of collision, the value of l_2 is 78 mm. The two motors move in two specified modes: 1) same direction with same speed; 2) opposite direction with same speed. The end effector will perform rotation motion and translation motion respectively. There are two constraints on the movement of the motors: 1) collision with the patient; 2) the limitation of α in (14).

B. Results

Figure 8 shows the validation results. In the first subplot, the tip of the end effector coincides with the RCM point when $\alpha = \alpha_1 = 10^\circ$. Maximum feed depth is reached when $\alpha = \alpha_2 = 80^\circ$ in the second subplot. To avoid the robot-patient collision, the point A'_1 and point A'_2 reach the limitation (human body), as shown in the third and fourth subplot, where the rotation angle is validated. So the working space of the designed mechanism is a sector, of which the radius is 47.8 mm and the arc angle is 90° .

VI. CONCLUSION

This paper developed a novel planar 1R1T RCM robot equipped with a novel three-rhombus mechanism. Design, kinematic modeling, and preliminary simulations were done

to establish and validate the proposed mechanism. The great merit of the mechanism is that the actuators which realize the 1R1T RCM are all mounted on the base. In addition, the two DOFs of the end effector can be decoupled, which simplifies the design of the controller further. Kinematic simulation is done preliminary to validate the correctness of the models. The results show that the optimized mechanism can realize the sector-shaped working space, of which the radius is 47.8 mm and the arc angle is 90° .

For further work, the dynamic model of the mechanism is supposed to be established and the controller needs to be designed to improve the accuracy of the RCM point.

REFERENCES

- [1] E. Franco, D. Brujic, M. Rea, W. M. Gedroyc, and M. Ristic, "Needle-guiding robot for laser ablation of liver tumors under mri guidance," *IEEE/ASME Transactions on Mechatronics*, vol. 21, no. 2, pp. 931–944, 2016.
- [2] S.-P. Ye, H. Qiu, S.-J. Liao, J.-H. Ai, and J. Shi, "Mini-invasive vs open resection of colorectal cancer and liver metastases: A meta-analysis," *World Journal of Gastroenterology*, vol. 25, no. 22, pp. 2819–2832, 2019.
- [3] W. Chen, S. Chen, J. Qu, and W. Chen, "A large-range compliant remote center of motion stage with input/output decoupling," *Precision Engineering*, vol. 51, pp. 468–480, 2018.
- [4] Z. Cui, W. Li, X. Zhang, P. W. Y. Chiu, and Z. Li, "Accelerated dual neural network controller for visual servoing of flexible endoscopic robot with tracking error, joint motion and rcm constraints," *IEEE Transactions on Industrial Electronics*, to be published, 10.1109/TIE.2021.3114674.
- [5] T. Kastritsi and Z. Doulgeri, "A controller to impose a rcm for hands-on robotic-assisted minimally invasive surgery," *IEEE Transactions on Medical Robotics and Bionics*, vol. 3, no. 2, pp. 392–401, 2021.
- [6] G. Chen, J. Wang, H. Wang, C. Chen, V. Parenti-Castelli, and J. Angeles, "Design and validation of a spatial two-limb 3rlt parallel manipulator with remote center-of-motion," *Mechanism and Machine Theory*, vol. 149, p. 103807, 2020.
- [7] Z. Wang, W. Zhang, and X. Ding, "Design and analysis of a novel mechanism with a two-dof remote centre of motion," *Mechanism and Machine Theory*, vol. 153, p. 103990, 2020.
- [8] Y. Jian, Y. Jin, M. Price, and J. Moore, "A new 7-degree-of-freedom 2-prrrr parallel remote center-of-motion robot for eye surgery," in *2020 8th IEEE RAS/EMBS International Conference for Biomedical Robotics and Biomechatronics (BioRob)*, 2020, pp. 891–896.
- [9] S. Shim, D. Ji, S. Lee, H. Choi, and J. Hong, "Compact bone surgery robot with a high-resolution and high-rigidity remote center of motion mechanism," *IEEE Transactions on Biomedical Engineering*, vol. 67, no. 9, pp. 2497–2506, 2020.
- [10] M. Afshar, J. Carriere, T. Meyer, R. Sloboda, S. Husain, N. Usmani, and M. Tavakoli, "Optimal design of a novel spherical scissor linkage remote center of motion mechanism for medical robotics," in *2020 IEEE/RSJ International Conference on Intelligent Robots and Systems (IROS)*, 2020, pp. 6459–6465.
- [11] S. Yoshida, T. Kanno, and K. Kawashima, "Surgical robot with variable remote center of motion mechanism using flexible structure," *Journal of Mechanisms and Robotics*, vol. 10, no. 3, 2018.
- [12] C.-B. Chng, B. Duan, and C.-K. Chui, "Modeling and simulation of a remote center of motion mechanism," in *2016 IEEE Region 10 Conference (TENCON)*, 2016, pp. 1755–1758.
- [13] L. Huang, Y. Yang, J. Xiao, and P. Su, "Type synthesis of 1rlt remote center of motion mechanisms based on pantograph mechanisms," *Journal of Mechanical Design*, vol. 138, no. 1, p. 014501, 2016.
- [14] W. Ye, B. Zhang, and Q. Li, "Design of a 1rlt planar mechanism with remote center of motion," *Mechanism and Machine Theory*, vol. 149, p. 103845, 2020.
- [15] L. Huang, L. Yin, B. Liu, and Y. Yang, "Design and error evaluation of planar 2dof remote center of motion mechanisms with cable transmissions," *Journal of Mechanical Design*, vol. 143, no. 1, 2021.